www.nature.com/aps

Acta Pharmacologica Sinica

ARTICLE

Ginsenoside 20(*S*)-Rh2 promotes cellular pharmacokinetics and intracellular antibacterial activity of levofloxacin against *Staphylococcus aureus* through drug efflux inhibition and subcellular stabilization

Xiao-yang Chen[1], Fei Qian[2], Yao-yao Wang[1], Yan Liu[1], Yuan Sun[1], Wei-bin Zha[1], Kun Hao[1], Fang Zhou[1], Guang-ji Wang[1] and Jing-wei Zhang[1]

Intracellular *Staphylococcus aureus* (*S. aureus*) often causes clinical failure and relapse after antibiotic treatment. We previously found that 20(*S*)-ginsenoside Rh2 [20(*S*)-Rh2] enhanced the therapeutic effect of quinolones in a mouse model of peritonitis, which we attributed to the increased concentrations of quinolones within bacteria. In this study, we investigated the enhancing effect of 20(*S*)-Rh2 on levofloxacin (LVF) from a perspective of intracellular bacteria. In *S. aureus 25923*-infected mice, coadministration of LVF (1.5 mg/kg, i.v.) and 20(*S*)-Rh2 (25, 50 mg/kg, i.g.) markedly increased the survival rate, and decreased intracellular bacteria counts accompanied by increased accumulation of LVF in peritoneal macrophages. In addition, 20(*S*)-Rh2 (1, 5, 10 μM) dose-dependently increased the uptake and accumulation of LVF in peritoneal macrophages from infected mice without drug treatment. In a model of *S. aureus 25923*-infected THP-1 macrophages, we showed that 20(*S*)-Rh2 (1, 5, 10 μM) dose-dependently enhanced the intracellular antibacterial activity of LVF. At the cellular level, 20(*S*)-Rh2 increased the intracellular accumulation of LVF by inhibiting P-gp and BCRP. PK–PD modeling revealed that 20(*S*)-Rh2 altered the properties of the cell but not LVF. At the subcellular level, 20(*S*)-Rh2 did not increase the distribution of LVF in lysosomes but exhibited a stronger sensitizing effect in acidic environments. Molecular dynamics (MD) simulations showed that 20(*S*)-Rh2 improved the stability of the DNA gyrase–LVF complex in lysosome-like acidic conditions. In conclusion, 20(*S*)-Rh2 promotes the cellular pharmacokinetics and intracellular antibacterial activities of LVF against *S. aureus* through efflux transporter inhibition and subcellular stabilization, which is beneficial for infection treatment.

Keywords: 20(*S*)-Rh2; levofloxacin; *Staphylococcus aureus*; intracellular bacteria; drug–drug interaction; cellular pharmacokinetics

Acta Pharmacologica Sinica (2021) 42:1930–1941; https://doi.org/10.1038/s41401-021-00751-z

INTRODUCTION

In 1916, Rous and Jones first proposed the concept that pathogenic microorganisms in cells evade the host immune response [1]. The "immune evasion" of bacteria into host cells is one of the main pathogeneses of infectious diseases. Intracellular bacteria may be protected from high concentrations of extracellular antibiotics, which in turn enhances the risk of developing drug resistance [2, 3]. For example, *S. aureus* invades many phagocytic and nonphagocytic cells, and intracellular *S. aureus* can be protected and proliferate in cells, escaping the immune response and antibiotic effects [4, 5]. Such intracellular *S. aureus* residual in tissues is associated with chronic or recurrent infections, including osteomyelitis [6], recurrent rhinosinusitis [7], pulmonary infections [8], and endocarditis [8, 9]. However, most antibiotics often have poor antibacterial activity against intracellular bacteria, leading to the formation of bacterial resistance [10]. Therefore, there is a pressing need to overcome the resistance of intracellular bacteria, and many reasonable strategies such as combined drug therapy have been proposed.

Ginsenoside 20(*S*)-Rh2 is an extremely low-content protopanaxadiol saponin extracted from red ginseng with various pharmacological activities and is extensively applied in the treatment of cancer [11], diabetes [12], ulcerative colitis [13], allergic disorders [14], etc. Our laboratory has studied ginsenoside 20(*S*)-Rh2 for a decade. Our previous studies showed that 20(*S*)-Rh2 was a noncompetitive inhibitor of P-gp, thereby increasing the intracellular concentrations and antitumor effects of adriamycin [15, 16]. Furthermore, we expanded the adjuvant therapy of 20(*S*)-Rh2 from tumor therapy to infection therapy. Single or multiple administrations of 20(*S*)-Rh2 enhanced the therapeutic effect of quinolones in a mouse peritonitis model, which was attributed to increased concentrations of quinolones within bacteria [17]. However, not only free bacteria but also intracellular bacteria are present in the peritonitis model, and these intracellular bacteria cause long-lasting and recurrent infections [18–20]. Therefore, we speculated that the significant enhancing effect of 20(*S*)-Rh2 towards antibiotics might also include actions towards intracellular bacteria.

[1]Key Lab of Drug Metabolism and Pharmacokinetics, China Pharmaceutical University, Nanjing 210009, China and [2]Affiliated Hospital of Nanjing University of Chinese Medicine, Nanjing 210023, China
Correspondence: Guang-ji Wang (guangjiwang@hotmail.com) or Jing-wei Zhang (zhangjw_cnnj@sina.com)
These authors contributed equally: Xiao-yang Chen, Fei Qian, Yao-yao Wang

Received: 19 January 2021 Accepted: 22 July 2021
Published online: 30 August 2021

LVF is a second-generation quinolone with strong, broad-spectrum antibacterial activity and can accumulate in cells, and the intracellular concentration at equilibrium is approximately twice that of the extracellular concentration [21]. Furthermore, LVF is a substrate for various types of efflux transporters, including P-gp, BCRP, and MRPs [10]. Therefore, this article intends to investigate the enhancing effect of 20(*S*)-Rh2 on LVF in a model of *S. aureus 25923*-infected THP-1 macrophages. The intracellular efficacy and concentrations of LVF in the absence or presence of 20(*S*)-Rh2 were compared, the main steps by which 20(*S*)-Rh2 participated and contributed to the enhancing effect were revealed by a PK–PD model and the possible efflux transporters involved were analyzed. Furthermore, the interactions of 20(*S*)-Rh2 and LVF were assayed at the lysosome level and interpreted by molecular dynamics (MD) simulations.

MATERIALS AND METHODS

Chemicals and reagents

Levofloxacin, gentamicin, MK571, sulfinpyrazone, KO143, quercetin, cyclosporine A, verapamil, and phorbol-12-myristate-13-acetate (PMA) were purchased from Sigma-Aldrich (St. Louis, MO, USA). 20(*S*)-Ginsenoside Rh2 (purity >98%) was purchased from Jilin University (Changchun, China). Mueller–Hinton (MH) broth and agar were obtained from Oxoid (Thermo Scientific, USA). FITC-*D*-Lys was purchased from Xiamen Bioluminor Bio-Technology Co., Ltd., (Xiamen, China). LysoTracker Red, acid phosphatase assay kit, and Hoechst 33342 were purchased from Beyotime Institute of Biotechnology (Haimen, China). Deionized water was prepared by a Milli-Q system (Millipore, Milford, MA, USA) and was used throughout.

Animals

Healthy ICR (CD-1) mice (18–22 g and 8–10 weeks, male and female in equal numbers) were obtained from Shanghai SLAC Laboratory Animal Co., Ltd. (Shanghai, China) and were kept eight per cage at room temperature (22 ± 1 °C) with 50%–60% relative humidity and an automatic day–night rhythm (12-h-cycle) in a clean-grade environment. Before each experiment, the animals were fasted overnight (12 h) with free access to water. All animal care and experimental procedures were conducted according to the National Research Council's Guidelines for the Care and Use of Laboratory Animals and were approved by the Animal Laboratory of China Pharmaceutical University (animal authorization reference number: SYXK2016-0011). Every effort was made to minimize animal pain, suffering, and distress and to reduce the number of animals used.

Survival assay and intracellular bacteria counting assay in mice

Since infection-caused mortality would lead to missing samples, the present study was divided into two parts. In the first experiment, 32 mice were used to establish the peritonitis model as described previously to determine the antibacterial effects in vivo [22]. In brief, *S. aureus 25923* suspensions (2×10^9 CFU/mL, 0.5 mL/mouse) were intraperitoneally injected into each mouse for infection. Then, they were randomly divided into four groups (eight mice per group): untreated group, LVF (1.5 mg/kg, i.v.) treatment group, LVF (1.5 mg/kg, i.v.) plus 20(*S*)-Rh2 (25 mg/kg, i.g.) treatment group, and LVF (1.5 mg/kg, i.v.) plus 20(*S*)-Rh2 (50 mg/kg, i.g.) treatment group. After drug administration, all the mice were monitored every 6 h for 24 h, the survival number in each group was recorded based on the observation of the natural death of the mice, and finally, a Kaplan–Meier survival curve was plotted. For the second experiment (intracellular bacteria counting assay), all conditions were the same as those in the first experiment, except that the concentration of bacteria inoculated into the mice was decreased to 4×10^8 CFU/mL to avoid massive death of mice in the untreated group 24 h postdrug administration, and correspondingly the dosage of LVF was descreased to 0.75 mg/kg. Peritoneal macrophages were prepared as we described previously [23], and intracellular bacteria counting was performed as mentioned later.

Accumulations of LVF in peritoneal macrophages of infected mice

On the one hand, mice infected with *S. aureus 25923* (2×10^9 CFU/mL, 0.5 mL/mouse) were treated with LVF (1.5 mg/kg, i.v.) alone, or LVF plus 20(*S*)-Rh2 (50 mg/kg, i.g.) as described in the above section, and peritoneal macrophages were collected 30 min after LVF administration for LVF determination. On the other hand, peritoneal macrophages were firstly prepared from infected mice without drug treatment, and then these cells were grouped and treated with LVF (4 μg/mL) alone or LVF plus 20(*S*)-Rh2 (1, 5, and 10 μM) for 6 and 12 h. Intracellular LVF concentrations were assayed with LC-MS/MS method.

Cell culture

THP-1 human peripheral blood monocytes were obtained from the American Type Culture Collection (Rockville, MD, USA) and cultured in RPMI-1640 medium supplemented with 10% fetal bovine serum (Invitrogen, Carlsbad, CA, USA) at 37 °C with 5% CO_2. The cell medium was changed every other day. To differentiate the suspended monocytes into adherent macrophages, THP-1 cells were incubated with PMA (150 ng/mL) in a complete medium for 48 h. All of the cells evaluated in this study were used between passages 10 and 20 and were negative for mycoplasma infection.

Bacterial strain and susceptibility testing

Staphylococcus aureus (*S. aureus*) strain ATCC 25923 was purchased from the American Type Culture Collection (Rockville, MD, USA). The bacteria were grown in MH broth at 37 °C with shaking (40×*g*). Colony-forming units (CFU) were counted on MH agar plates. *S. aureus 25923* suspensions were loaded onto an automatic microplate reader, and the optical density at 600 nm (OD_{600}) was measured. Minimum inhibitory concentrations (MICs) were determined by serial twofold microdilution according to the US National Committee for Clinical Laboratory Standards. Minimum bactericidal concentrations (MBCs) were defined as the lowest concentration of a drug that did not permit any visible growth (>99.9% reduction) on the plates after incubation at 37 °C overnight.

Extracellular antibacterial assays in broth

Logarithmic-phase bacteria were suspended in MH broth at 10^6 CFU/mL and exposed to various concentrations of LVF for a designated time at 37 °C. Then, the number of viable bacteria was counted by MH agar plate assays with appropriate dilution. For antibiotic-containing culture samples, sufficient dilution was performed to minimize antibiotic carryover to the MH agar plate.

Intracellular infection

Intracellular infection was performed as described previously with minor modifications [24]. Briefly, PMA-induced adherent THP-1 cells were exposed to *S. aureus 25923* at a multiplicity of infection (MOI) of 100:1 in a volume of 1 mL per well for 1 h at 37 °C in a 5% CO_2 incubator. Then, the bacteria-containing medium was discarded, and the infected cells were washed with prewarmed phosphate-buffered saline (PBS), followed by incubation with gentamicin (50 μg/mL, at least six times higher than the MBC of gentamicin in broth) for 1.5 h to eradicate extracellular bacteria. Subsequently, the cells were washed again and incubated continuously with gentamicin (2 μg/mL, the MIC of gentamicin in broth), which provides adequate protection against the extracellular growth of *S. aureus 25923* up to 24 h.

Morphological studies of intracellular bacteria

S. aureus 25923 was first labeled with FITC-*D*-Lys as described previously [25] and then used to infect THP-1 cells. Before observation, the nuclei and lysosomes of infected THP-1 cells were dyed with Hoechst 33342 and LysoTracker Red, respectively. A confocal laser scanning microscope (FV3000, Olympus, Japan) was used to observe the location of *S. aureus 25923* (green fluorescence) within THP-1 cells (nuclei: blue fluorescence; lysosomes: red fluorescence).

For electron microscopy observation, *S. aureus 25923* (unlabeled)-infected THP-1 cells were collected and fixed with 2.5% glutaraldehyde in 0.1 M phosphate buffer at 4 °C. After washing, the samples were fixed with 1% osmium tetroxide. Ultrathin sections were stained with uranyl acetate and lead citrate. Finally, the ultrastructures were observed under a transmission electron microscope (JEM-1011, JEOL, Japan).

Intracellular antibacterial assays in THP-1 macrophages

Infected adherent THP-1 cells were incubated with various concentrations of LVF at different times. After washing with PBS, the cells were suspended in sterile water, followed by vigorous shaking for 30 s to fully lyse the cells. Aliquots were then plated on MH agar after appropriate dilution. The number of CFU was counted after incubation at 37 °C for 24 h.

Intracellular accumulation and lysosome distribution studies

Intracellular accumulation studies were performed as we described previously [24]. In brief, the cells were treated with drugs at 37 °C for the designated time. Then, the cells were washed with ice-cold PBS and collected, followed by sonication to achieve homogeneity. Aliquots were used to determine drug concentrations. All experiments were conducted in triplicate.

For the lysosome distribution study, the lysosomes of THP-1 cells were isolated according to the literature, with minor modifications [6–8]. Briefly, 10^8 cells were disrupted with a Dounce glass homogenizer, followed by centrifugation at 800×*g* for 10 min to remove the nuclei and cellular debris. Then, the supernatants were collected and centrifuged at 20,000×*g* for 10 min to pellet lysosomes. The resulting pellet was loaded on top of a discontinuous density gradient of Optiprep™ and subjected to ultracentrifugation at 100,000×*g* for 1 h, and the top band of the tube was collected as the lysosome fractions. The lysosomes were identified by acid phosphatase assay kit (Beyotime Institute of Biotechnology, Haimen, China) for its biomarker enzyme, and observed by confocal laser scanning microscope for its staining with LysoTracker Red. Subsequently, two schemes, namely, drug treatment first and then lysosome collection or lysosome collection first and then drug treatment, were performed. Then, the lysosomes were washed and ultrasonically broken to determine the LVF concentration. Protein calibration further ensured the accuracy of drug concentration determination.

Efflux transporter membrane vesicle transport assay

Human BCRP and MRP2-expressing membrane vesicle transport assays were performed according to the manufacturer's instructions with minor modifications (GenoMembrane Co., Ltd, Japan). The test compound 20(*S*)-Rh2 and substrate probe (10 μM Lucifer yellow for BCRP; 50 μM estradiol-17β-*D*-glucuronide for MRP2) were added to the transport medium and preincubated at 37 °C for 5 min. Then, this solution was mixed rapidly with a reaction mixture for another 5 min incubation. Ice-cold wash buffer was added to stop the reactions. Lucifer yellow was quantitated by an automatic microplate reader (Synergy H1, BioTek, Vermont, USA) at excitation wavelength of 428 nm and emission wavelength of 536 nm. Estradiol-17β-*D*-glucuronide was determined by LC-MS/MS as we described previously [26].

Efflux transporter gene expression assay

THP-1 cells were incubated with 20(*S*)-Rh2 (1, 5, and 10 μM) for 24 h, and then, cells were collected and suspended in a High Pure RNA Isolation Kit (RNAiso Plus, Takara Bio, Japan). Total RNA was extracted. Then, the RNA was reverse-transcribed into cDNA with a PrimeScript RT Regent Kit (Takara Bio, Japan). Quantitative real-time PCR (qPCR) was performed in a real-time RT-PCR detection system (CFX96, Bio-Rad, California, USA). The primers for efflux transporters were the same as those described previously [26].

Determination of drug concentrations

LVF was measured with a liquid chromatography (LC20A, Shimadzu, Japan)-tandem mass spectrometry (Triple Quad 6500, SCIEX, Massachusetts, USA) system. Briefly, samples were protein-precipitated with two volumes of acetonitrile containing zolpidem as an internal standard (IS). After centrifugation, the supernatant was injected into the system and separated on a Waters XSelect HSS T3 column (3.0 mm × 50 mm, 2.5 μm, Waters, Massachusetts, USA). The mobile phase consisted of water containing 0.1% formic acid (A) and acetonitrile (B) with the following gradient: 0 min, 5% B; 1.5 min, 5% B; 3.5 min, 40% B; 5.5 min, 40% B; 6.5 min, 90% B; 8 min, 90% B; 8.5 min, 5% B; and 10 min, 5% B. The flow rate was 0.3 mL/min. Mass spectrometer detection was performed in positive electrospray ionization (ESI) mode. The declustering potential was 60 V for LVF and 70 V for IS. The collision energy was 25 eV for LVF and 30 eV for the IS. Quantification was performed using multiple reaction monitoring modes: *m/z* 362.4→318.2 for LVF and *m/z* 308.2→235.2 for the IS.

Molecular dynamics (MD) simulation of LVF and DNA gyrase

Generally, the operation process was divided into two steps. First, the complex of LVF and DNA gyrase (PDB ID: 2XCT) was prepared by molecular docking using AutodockTools, with which LVF was docked into the active sites (grid box size 45 Å × 45 Å × 45 Å with grid spacing 0.375 Å) of protonated DNA gyrase in different environments. Docking was performed using the Lamarckian genetic algorithm, of which the altered parameters were the population size (150), the maximum number of evaluations (25,000,000), and the maximum number of generations (27,000), and all other parameters were kept as default. After the docking simulation was complete, the lowest energy conformation output was considered the initial conformation for the subsequent MD studies.

MD simulation of the DNA gyrase and LVF complex in the physiological environment system was carried out by Amber V16 with an amber99 force field. NaCl (0.9%) was added to the system, and the pH value was adjusted to 5.2 or 7.2. Before free MD simulation, the complex system was refined through 2000 steps of the steepest descent method, followed by solvent MD simulation, keeping the protein and LVF fixed for 100 ps. Then, MD simulation was performed twice for 100 ps with the main chain or the C*a* of the protein and the ligand fixed. Finally, a 3 ns MD simulation without restriction was carried out at 1 bar and 300 K, with a 1.4 nm cut-off for van der Waals interactions. An all-bond constraint was used to keep the ligand from drifting during MD simulation. The equation of motions was integrated with a 1 fs time step, and the atomic coordinates were recorded to the trajectory file every 2.5 ps for later analysis.

PK–PD model

LVF uptake kinetics were modeled using a one-compartment absorption model, and a sigmoid maximum effect (E_{max}) model was introduced as a pharmacodynamic model. A brief schematic presentation of this model is shown in Fig. 1, where X_1 and X_2 are the amounts of LVF in the cell culture well and within the cell, respectively, and k and F_a are the uptake transport constant and accumulation fraction of LVF across the cell membrane,

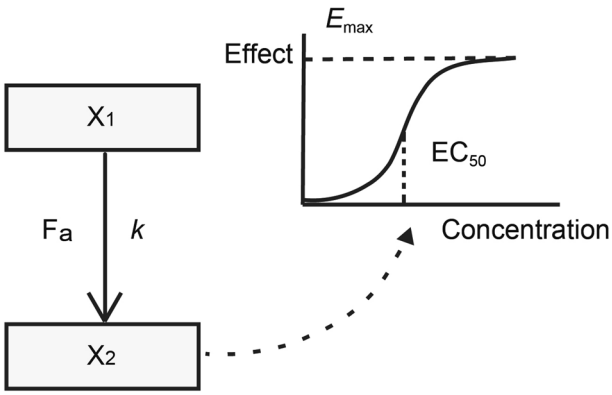

Fig. 1 A brief schematic presentation of the cellular PK–PD model. LVF uptake kinetics were modeled using a one-compartment absorption model, and a sigmoid E_{max} model was introduced as a pharmacodynamic model. X_1 and X_2 are the amounts of LVF in the cell culture well and within the cell, respectively. k and F_a are the uptake transport constant and accumulation fraction of LVF across the cell membrane, respectively. E_{max} is the difference in effect between the greatest amount of growth (as seen for the growth control, E_0) and the greatest amount of killing. EC_{50} is the concentration value producing a 50% reduction in intracellular bacterial counts.

respectively. E_{max} is the difference in effect between the greatest amount of growth (as seen for the growth control, E_0) and the greatest amount of killing. EC_{50} is the concentration value producing a 50% reduction in intracellular bacterial counts. An integrated PK–PD model was constructed as differential functions with Eqs. (1)–(4). All parameters were estimated by ADAPT 5 software.

$$\frac{dX_1}{dt} = -k * X_1 \quad (1)$$

$$\frac{dX_2}{dt} = k * X_1 \quad (2)$$

$$c = \frac{k * X_1 * F_a}{V} \quad (3)$$

$$\frac{dE}{dt} = \frac{E_{max} * c}{EC_{50} + c} \quad (4)$$

Data analysis

The data are expressed as the mean ± SEM. The statistical analyses included two-tailed Student's *t*-test and one-way ANOVA. The difference was considered to be statistically significant if the probability value was less than 0.05 ($P < 0.05$).

RESULTS

20(*S*)-Rh2 increased the survival rate and decreased intracellular bacteria counts in *S. aureus 25923*-infected mice

The *S. aureus 25923*-induced model mice all died within 16 h without drug treatment (Fig. 2a). Moreover, the model mice treated with 1.5 mg/kg LVF achieved an ~25% survival rate. When 20(*S*)-Rh2 (50 mg/kg) was combined with LVF (1.5 mg/kg), the survival rate was markedly extended to 50%, which was twice that in the LVF group and significantly better than that in the untreated group ($P = 0.0252$). Meanwhile, the intracellular bacteria counts in peritoneal macrophages were significantly decreased in the LVF plus 20(*S*)-Rh2 groups compared with the untreated group (Fig. 2b).

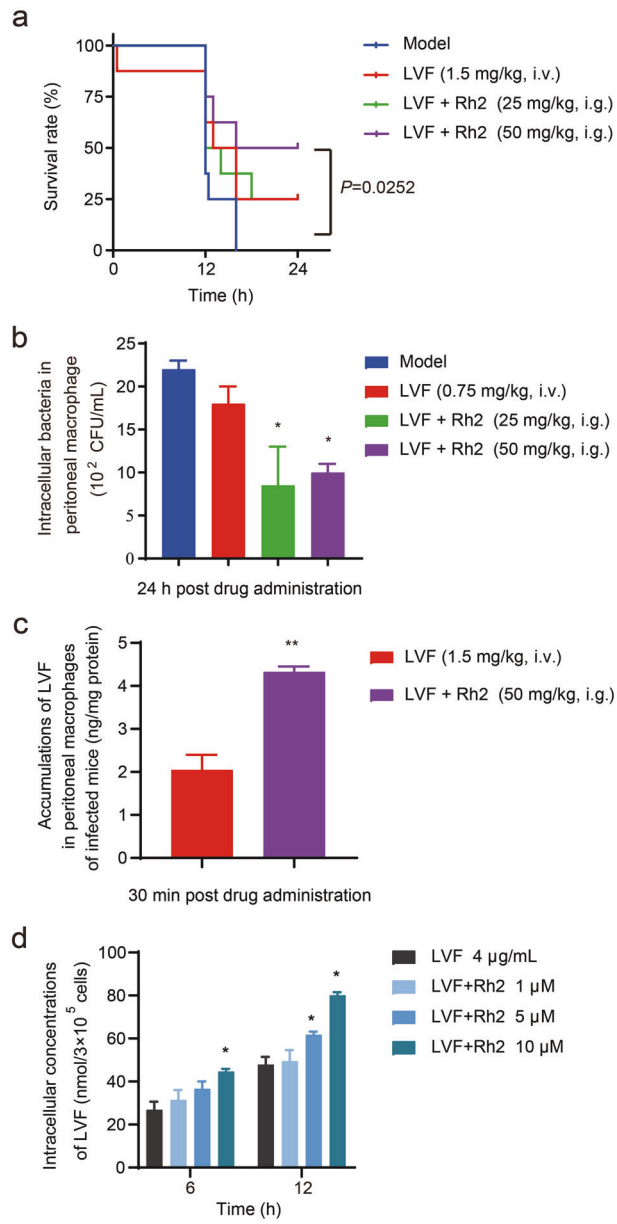

Fig. 2 20(*S*)-Rh2 increased the survival rate and decreased intracellular bacteria counts in *S. aureus* 25923-infected mice with increased intracellular LVF concentrations in peritoneal macrophages. An *S. aureus 25923* suspension was intraperitoneally injected into each mouse for infection. Then, the mice were randomly divided into four groups: untreated group, LVF treatment group, LVF plus 20(*S*)-Rh2 (25 mg/kg, i.g.) treatment group, and LVF plus 20(*S*)-Rh2 (50 mg/kg, i.g.) treatment group. **a** After drug administration, all the mice were monitored every 6 h for 24 h. The survival number in each group was recorded based on the observation of the natural death of the mice, and finally, a Kaplan–Meier survival curve was plotted. **b** Peritoneal macrophages were collected and prepared 24 h postdrug administration, and intracellular bacteria were counted. **c** Peritoneal macrophages were collected and prepared 30 min postdrug administration, and intracellular concentrations of LVF in peritoneal macrophages were determined by LC-MS/MS. **d** Peritoneal macrophages of infected mice without drug treatment were prepared and treated with LVF (4 μg/mL) or LVF plus 20(*S*)-Rh2 (1, 5, and 10 μM), and intracellular concentrations of LVF were determined by LC-MS/MS. The model group (no drug treatment) was used as a control for (**a**) and (**b**), and a single dose of LVF was used as a control for (**c**) and (**d**). The significance is indicated by $^*P < 0.05$, $^{**}P < 0.01$ versus the control.

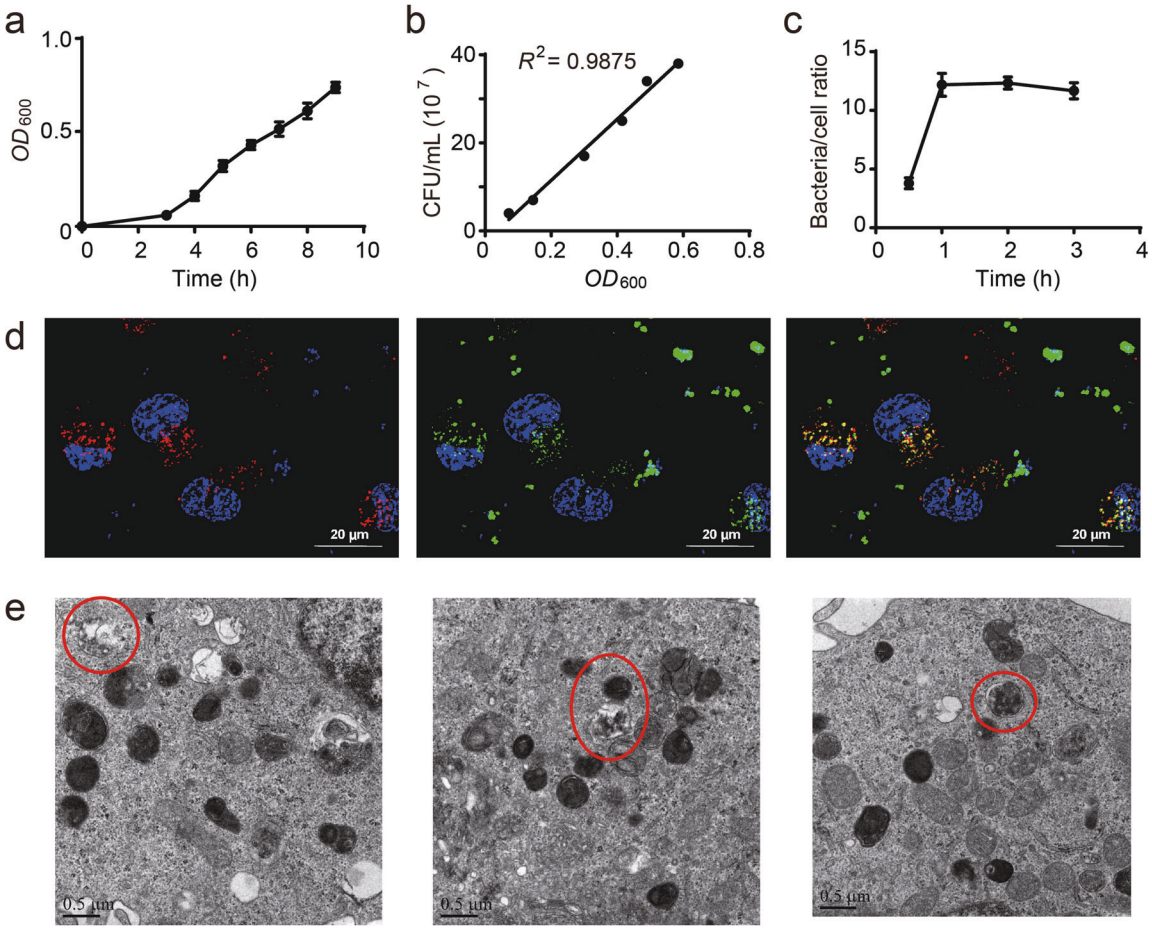

Fig. 3 Development of the model of *S. aureus* 25923-infected THP-1 macrophages. a Growth curve of *S. aureus 25923*. **b** Correlation of the *OD* value and number of CFU of *S. aureus 25923* from 3 to 8 h. **c** Time-dependent bacteria/cell ratio. Cells were incubated for 0.5, 1, 2, and 3 h with *S. aureus 25923*, and data were presented as the mean ± SEM, $n = 3$. **d** Confocal laser scanning microscopy observation of *S. aureus 25923*-infected THP-1 cells. *S. aureus 25923* was labeled with FITC-*D*-Lys (green fluorescence) and then used to infect THP-1 cells, in which the nuclei and lysosomes were dyed with Hoechst 33342 (blue fluorescence) and LysoTracker Red (red fluorescence), respectively. Yellow fluorescence indicated the colocalization of green fluorescence and red fluorescence. **e** Transmission electron microscopy observation of infected THP-1 cells. Red circles: *S. aureus 25923* was captured by phagocytic vesicles, fused with lysosomes, and finally located within lysosomes.

20(*S*)-Rh2 increased intracellular accumulations of LVF in peritoneal macrophages

When infected mice were treated with LVF in the presence of 20(*S*)-Rh2, the accumulations of LVF in peritoneal macrophages were significantly increased by twofold compared with those treated with LVF alone (Fig. 2c). Furthermore, peritoneal macrophages of infected mice without drug treatment were prepared in advance, and then the uptake and accumulation of LVF was also increased by 20(*S*)-Rh2 in a concentration-dependent manner (Fig. 2d).

Development of the *S. aureus 25923*-infected THP-1 macrophage model

Under our culture conditions, the growth of *S. aureus 25923* reached logarithmic phase after 4 h of incubation (Fig. 3a), and the linearity between the OD value and number of CFU was quite good during 3 to 8 h of culture time, with $R^2 = 0.9875$ (Fig. 3b). Then, MOI values of 10:1, 20:1, and 100:1 were tested in PMA-induced adherent THP-1 cells, of which the intracellular *S. aureus* 25923 counts were ~0.08, 1, and 11 CFU/cell, respectively (Table 1), and finally, an MOI of 100:1 was chosen. Subsequently, the infection time of 1 h was selected because the intracellular *S. aureus 25923* concentration was saturated after 1 h (Fig. 3c). As shown in Fig. 3d, when *S. aureus 25923* was introduced, its green fluorescence could be found not only outside cells as free bacteria (far from the blue fluorescence of nuclei) but also colocalized with the red fluorescence of lysosomes within cells and merged as yellow fluorescence. Furthermore, *S. aureus 25923* was also observed being captured by phagocytic vesicles, fused with lysosomes, and finally located within lysosomes by transmission electron microscopy, which was pointed out by the red circles in Fig. 3e.

Table 1. Intracellular bacteria/cell ratio of different MOI.

MOI	10:1	20:1	100:1
Intracellular bacteria/cell	0.08	1	11

Decreased susceptibility of intracellular *S. aureus 25923* to LVF

As shown in Fig. 4a, 0.5, 1, 2, 4, and 8 μg/mL LVF appreciably inhibited the growth of *S. aureus 25923* in broth in a concentration-dependent manner. At a concentration of 8 μg/mL for 5 h, LVF decreased *S. aureus* 25923 in broth by $3\Delta Log_{10}$. However, when *S. aureus 25923* invaded the THP-1 macrophages, they became resistant to LVF, as even 16 μg/mL LVF exhibited a weak inhibitory effect (only $0.7\Delta Log_{10}$ decrease) against *S. aureus*

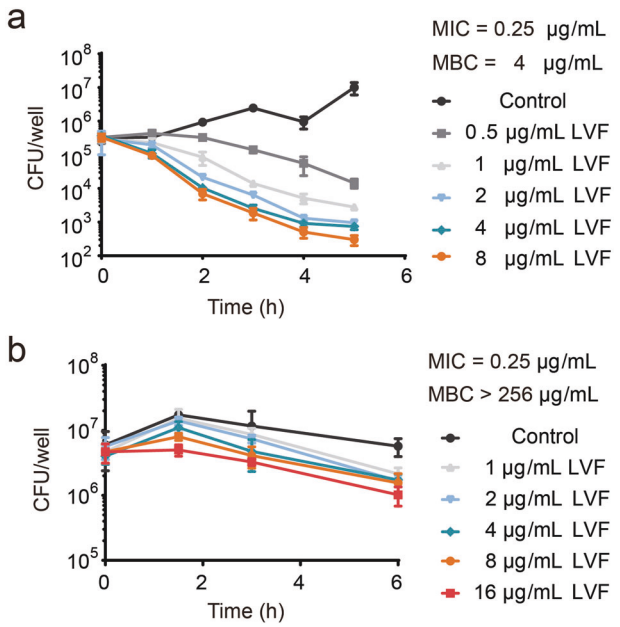

Fig. 4 Differences in the extracellular and intracellular antibacterial effects of LVF. a Extracellular curve of LVF against *S. aureus 25923*. Logarithmic-phase bacteria were suspended in MH broth at 10^6 CFU/mL and exposed to various concentrations of LVF for the designated time at 37 °C. Then, the number of viable bacteria was counted by MH agar plate assays with appropriate dilution. **b** The intracellular killing curve of LVF against *S. aureus 25923*. Infected adherent THP-1 cells were incubated with various concentrations of LVF at different times. After washing with PBS, the cells were suspended in sterile water, followed by vigorous shaking to fully lyse the cells. Aliquots were then plated on MH agar after appropriate dilution. The number of CFU was counted after incubation at 37 °C for 24 h.

25923 after 6 h of incubation (Fig. 4b). The MIC and MBC of LVF against *S. aureus* 25923 in broth and infected THP-1 macrophages were also determined, and the MBC of LVF against intracellular *S. aureus 25923* increased markedly, far beyond 256 μg/mL.

20(*S*)-Rh2 enhanced both intracellular antibacterial effects and intracellular accumulation of LVF by efflux transporter inhibition

As shown in Fig. 5a, compared to LVF treatment alone (three concentration levels), the combination of 20(*S*)-Rh2 and LVF significantly reduced the number of live bacteria in THP-1 macrophages in a concentration-dependent manner. In particular, 10 μM 20(*S*)-Rh2 combined with 4 μg/mL LVF sharply reduced the number of intracellular residual viable *S. aureus 25923* cells to 0.48-fold that with LVF single treatment. Regarding the time-dependent kinetics, 20(*S*)-Rh2 (10 μM) began to enhance the intracellular antibacterial effects of LVF at 3 h after drug treatment, and 5 μM 20(*S*)-Rh2 also exhibited an enhancing effect after 6 h of treatment together with LVF (Fig. 5b). However, 20(*S*)-Rh2 itself had no significant bactericidal effect when compared with the control group (Fig. 5c). Moreover, 20(*S*)-Rh2 was observed to significantly increase the accumulation of LVF in THP-1 macrophages in a concentration- and time-dependent manner, and 10 μM 20(*S*)-Rh2 increased LVF accumulation up to 2.86-fold after 6 h of combination treatment (Fig. 5d). At 37 °C, the uptake of LVF in THP-1 macrophages reached 14.88 ng/mg protein. When the incubation was set to 4 °C, the uptake of LVF notably increased to 41.96 ng/mg protein. Furthermore, the addition of 20(*S*)-Rh2 markedly increased the uptake of LVF by THP-1 macrophages at 37 °C in a concentration-dependent manner, while there was no significant change in the presence of 20(*S*)-Rh2 at 4 °C (Fig. 5e). Subsequently, various types of efflux transporter inhibitors all significantly increased the accumulation of LVF in THP-1 macrophages (Fig. 5f). As shown in Fig. 5g, 20(*S*)-Rh2 exhibited a moderate inhibitory effect on human BCRP, with an IC_{50} of 20.32 μM. However, 20(*S*)-Rh2 did not obviously inhibit MRP2 (Fig. 5h). Furthermore, there was no significant change in BCRP, MRP2, and P-gp expression in THP-1 cells after 20(*S*)-Rh2 treatment for 24 h (Fig. 5i).

Elevated accumulation fraction of LVF in THP-1 macrophages contributed mainly to the enhanced intracellular antibacterial effect of LVF by 20(*S*)-Rh2

As shown in Fig. 6, the fitting results matched reasonably well with the measured values. When LVF treatment was combined with 20(*S*)-Rh2, the accumulation fraction (F_a) was significantly increased by approximately twofold (Table 2). However, 20(*S*)-Rh2 did not influence the uptake transport constant *k* of LVF across the cell membrane or the efficacy of LVF itself (E_{max} and EC_{50}).

20(*S*)-Rh2 exhibited a stronger sensitizing effect towards LVF under lysosome-like acidic conditions

The prepared lysosomes were identified with extremely high acid phosphatase activity which is a biomarker enzyme of lysosomes (Fig. 7a). Meanwhile, the prepared lysosomes were also labeled with LysoTracker Red and observed as a cluster form with a confocal laser scanning microscope (Fig. 7b). When THP-1 macrophages were incubated with LVF in the presence or absence of 20(*S*)-Rh2 for 2 h, lysosomes were isolated, and there was no change in LVF accumulation in lysosomes between the two groups (Fig. 7c). Moreover, lysosomes of THP-1 macrophages were isolated beforehand and directly incubated with LVF plus or minus 20(*S*)-Rh2, and there was no significant change (Fig. 7d). As a matter of fact, the susceptibilities of *S. aureus 25923* to LVF varied with the alteration in pH values (Table 3). Under lysosome-like acidic conditions (pH 5.2), both the MIC and MBC were higher than those under neutral conditions (pH 7.2). When 20(*S*)-Rh2 was added together with LVF under both pH 5.2 and pH 7.2 incubation conditions, the susceptibilities of *S. aureus 25923* to LVF were all markedly increased. In particular, 20(*S*)-Rh2 together with LVF inhibited *S. aureus 25923* more significantly at pH 5.2 than at pH 7.2 and restored the susceptibility of *S. aureus 25923* at pH 5.2 to that observed at pH 7.2 (Fig. 7e).

20(*S*)-Rh2 strengthened the MD stability of LVF under acidic conditions

As shown in Fig. 8a, the root-mean-square deviation (RMSD) curves of the DNA gyrase–LVF complex fluctuated markedly at the initial stage of MD simulation until 1500 ps, which was due to the self-adjustment and self-adaptation of the DNA gyrase structure caused by the solvation effect of the complex. After equilibrium, the RMSD curves of the DNA gyrase–LVF complex in different pH environments were markedly distinguished. The RMSD value was below 3.5 Å at pH 7.2, while it was above 4.5 Å at pH 5.2 (Fig. 8a). Moreover, DNA gyrase exhibited a much lower electrostatic energy at pH 7.2 than at pH 5.2 (Fig. 8c). When 20(*S*)-Rh2 was added to the pH 5.2 environment, it significantly lowered the RMSD value from 4.5 to 3.5 Å (Fig. 8b) and decreased the energy from -3.8×10^6 kJ/mol to -4.1×10^6 kJ/mol (Fig. 8d).

DISCUSSION

S. aureus is one of the main leading causes of bacterial infections in humans worldwide and represents a major health problem in hospital and community settings [27–29]. *S. aureus* can easily adhere to and invade phagocytic or nonphagocytic cells [21, 30]. In phagocytic cells, *S. aureus* often survives in vacuolar compartments in a semidormant state and escapes phagocytic cells to establish infections [31, 32]. This form of cell presence causes recurrent episodes of the well-known *S. aureus* infectious disease and leads

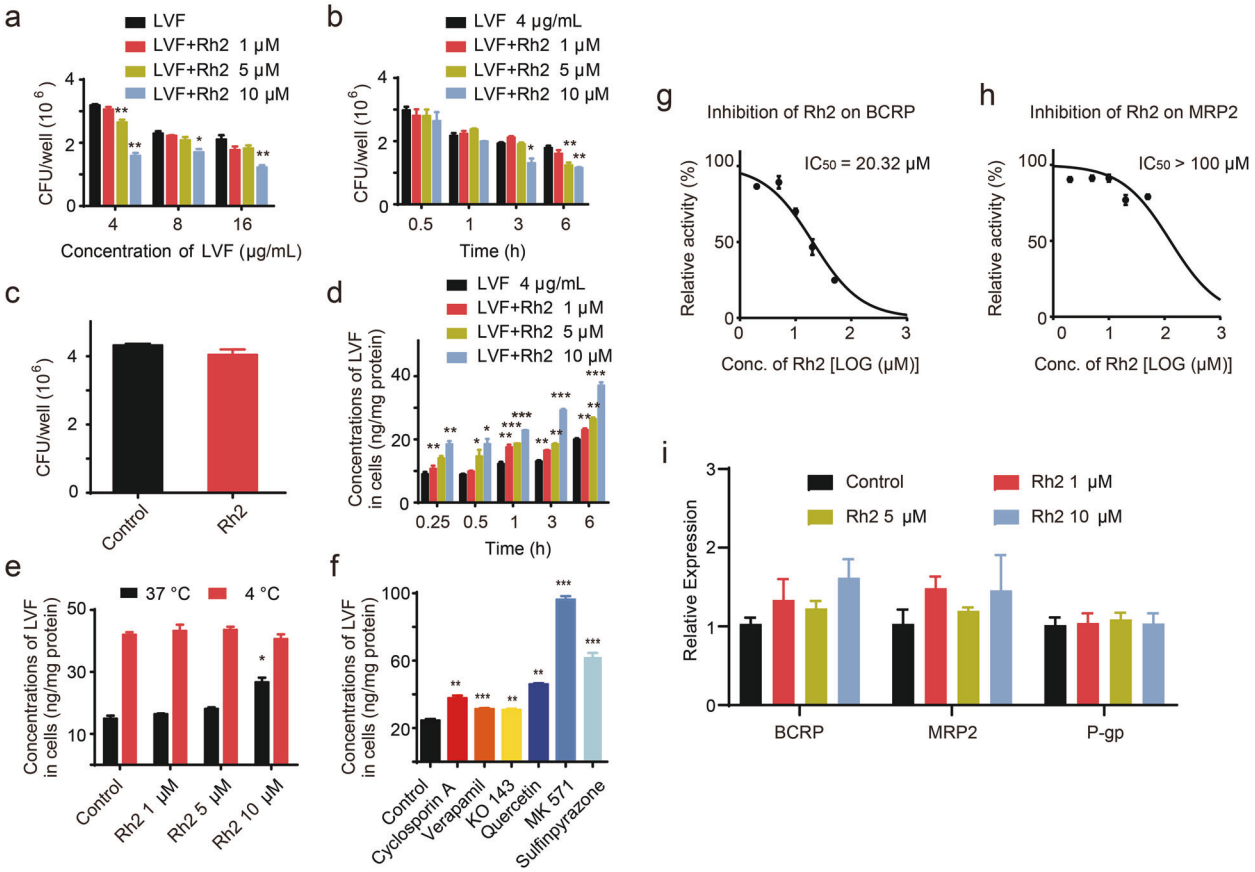

Fig. 5 20(*S*)-Rh2 enhanced the intracellular antibacterial effects and accumulation of LVF by efflux transporter inhibition in vitro. a Number of intracellular *S. aureus 25923* after 6 h of incubation with 20(*S*)-Rh2 and LVF. Infected cells were preincubated with 20(*S*)-Rh2 for 0.5 h followed by further incubation for 6 h in the presence of 4, 8, and 16 μg/mL LVF. **b** Number of intracellular *S. aureus 25923* after incubation with 20(*S*)-Rh2 and LVF. Infected cells were preincubated with 20(*S*)-Rh2 for 0.5 h followed by further incubation for 0.5, 1, 3, and 6 h in the presence of 4 μg/mL LVF. **c** Number of intracellular *S. aureus 25923* in infected cells after incubation with 20(*S*)-Rh2 alone (10 μM) for 6 h. **d** Effects of 20 (*S*)-Rh2 on the accumulation of LVF in THP-1 macrophages. Cells were preincubated with 20(*S*)-Rh2 for 0.5 h followed by further incubation for 0.25, 0.5, 1, 3, and 6 h in the presence of 4 μg/mL LVF. **e** Cellular accumulation of LVF in THP-1 macrophages under different temperature conditions (37 and 4 °C) with or without 20(*S*)-Rh2. Cells were preincubated with 20(*S*)-Rh2 for 0.5 h under different temperature conditions followed by further incubation for 3 h in the presence of 4 μg/mL LVF. **f** Effects of P-gp, BCRP, and MRP2 inhibitors on the cellular accumulation of LVF in THP-1 macrophages. Cells were preincubated with cyclosporin A (20 μM), verapamil (50 μM), MK571 (5 μM), sulfinpyrazone (500 μM), Ko143 (2 μM), and quercetin (10 μM) for 0.5 h followed by a further 3-h incubation in the presence of 4 μg/mL LVF. **g**, **h** Inhibitory effect of 20 (*S*)-Rh2 on the activity of human BCRP and MRP2. 20(*S*)-Rh2 and substrate probe (10 μM Lucifer yellow for BCRP; 50 μM estradiol-17β-*D*-glucuronide for MRP2) were added to the corresponding membrane vesicles and preincubated at 37 °C for 5 min, followed by rapid mixing with the reaction mixture for another 5 min incubation. **i** Effects of 20(*S*)-Rh2 on the expression of efflux transporters in THP-1 cells. THP-1 cells were incubated with 20(*S*)-Rh2 (1, 5, and 10 μM) for 24 h and then collected for quantitative real-time PCR assay. The data were presented as the mean ± SEM, $n = 3$. A single dose of LVF was used as a control for (**a**), (**b**), (**d**), (**e**), and (**f**), and the no drug treatment group was used as a control for (**c**), and (**i**). The significance is indicated by $^{*}P < 0.05$, $^{**}P < 0.01$, $^{***}P < 0.001$ versus the control.

to the failure of common antibiotic treatment [33, 34]. Therefore, only if antibiotics at a sufficient amount and efficacy can penetrate and reside within *S. aureus*-infected cells can intracellular bacteria be cleared out. Intracellular drug concentration and efficacy have become important parameters and focuses for new drug candidate evaluations and drug therapy designs [35–37].

Human THP-1 monocytes have been widely used for intracellular antibacterial assays [38–40] and were selected to establish an *S. aureus 25923*-infected cell model in our research. During the logarithmic growth phase of *S. aureus 25923*, the linearity was good between the number of CFU and *OD* values, which made it easy to use the *OD* value to control bacterial density throughout the experiments. How can bacteria be efficiently introduced into THP-1 cells? For full internalization, most pathogens including *S. aureus 25923* produce a wall-associated protein called adhesin, which can interact with the host receptor, utilize and induce the host's signaling pathway, and directly cause rearrangement of the host's cytoskeleton [41, 42]. Among these proteins, it has been suggested that anchored collagen adhesin plays important role in *S. aureus 25923* host adherence [43]. However, it is not always "the more, the better". When too much *S. aureus 25923* actively proliferates in cells, the cells would be dissolved and die. Hence, the appropriate time, bacterial dose, and temperature are crucial for this infection. After several trials, when the MOI was 100:1 and the infection time was 1 h, an average of 11 CFU of bacteria invaded each THP-1 cell. To eliminate uninfected excessive bacteria, 50 μg/mL gentamicin for 1.5 h was used to remove extracellular bacteria, and 2 μg/mL gentamicin was used to maintain this status for 24 h [44, 45]. As shown in Fig. 3d, e, *S. aureus 25923* was captured into phagocytic vesicles, fused with lysosomes, and finally located within lysosomes. This observation indicated that *S. aureus 25923* could survive in the cell and could grow and reproduce [5, 46, 47], which contributed to the persistence and recurrence of infection [30, 48]. This finding was further demonstrated by subsequent experiments.

The MBCs of LVF on extracellular and intracellular *S. aureus 25923* were largely different [49]. Even if the concentration of LVF was greater than 256 μg/mL, LVF could not completely kill intracellular bacteria. In contrast, only 4 μg/mL LVF was necessary to kill extracellular bacteria in broth. This phenomenon has also been observed for some other antibacterial drugs against intracellular infections [50]. Further detailed analysis of the bactericidal capacity of LVF was performed to map the time-sterilization curves of extracellular (Fig. 4a) and intracellular (Fig. 4b) bacteria, and the results suggested that the time and efficiency of intracellular killing of LVF was much lower than that of extracellular bacteria. Why did there exist so sharp a difference in the efficacy of LVF? The bacteria just resided in different environments [21]. Extracellular bacteria might be exposed to sufficient LVF in the plasma directly. For intracellular bacteria, however, the cell membrane seems to be a wall that weakens the attack of LVF in terms of action time and strength. Therefore, targeting the wall and allowing more LVF to accumulate within the cells might be a strategy to enhance the intracellular antibacterial efficacy [39]. Many drugs have been found to facilitate the entry of antibiotics into infected cells. For example, Seral et al. confirmed that the P-gp inhibitor verapamil enhanced the killing effect of azithromycin against *Listeria* and *Staphylococcus aureus* in murine J774 cells [5].

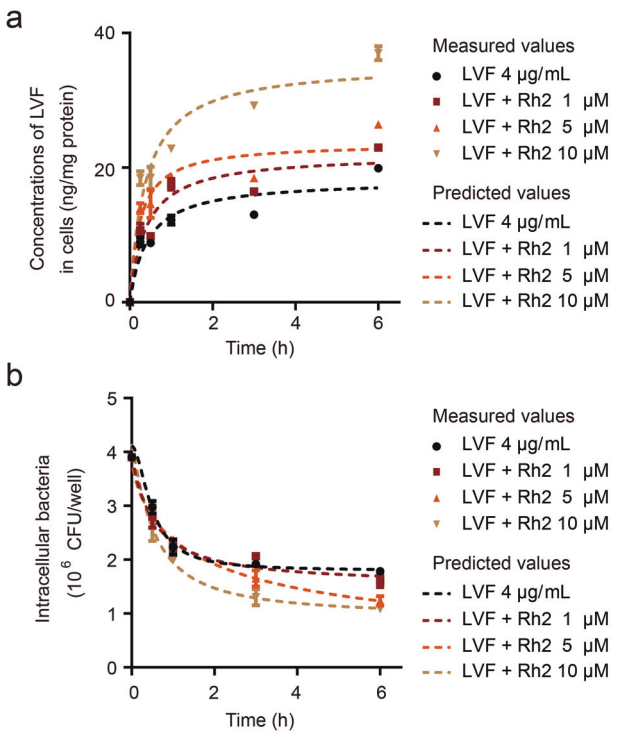

Fig. 6 The increased absorption fraction of LVF in THP-1 macrophages contributed mainly to the enhanced intracellular antibacterial effect of LVF by 20(*S*)-Rh2. The PK–PD model described the uptake kinetics of LVF (**a**) and its intracellular antibacterial effect (**b**) with or without 20(*S*)-Rh2 in THP-1 macrophages. The dotted lines are the predicted values, and the nearby points are the measured values.

A nontoxic dose of 20(*S*)-Rh2 can increase the efficacy of antitumor drugs when combined with some common antitumor drugs including anthracyclines through inhibition of P-gp [15, 16, 51, 52]. Many antibiotics are actively effluxed by efflux transporters [4, 5, 53]. Therefore, it has been speculated that inhibition of the corresponding efflux transporter can increase the intracellular content of the drug, thereby enhancing the intracellular activity of the drug [53, 54]. In the treatment of intracellular infections, the intracellular enhancing effect of 20(*S*)-Rh2 on antibacterial drugs has not been reported. In our experiment, 20(*S*)-Rh2 plus LVF increased the survival rate of *S. aureus* 25923-infected mice in vivo, with decreased intracellular bacterial counts and increased intracellular LVF concentrations in peritoneal macrophages (Fig. 2). Furthermore, 20(*S*)-Rh2 increased the intracellular bactericidal activity of LVF in a concentration- and time-dependent manner in vitro (Fig. 5a, b). However, in the model of *S. aureus 25923*-infected THP-1 macrophages, a single dose of 20(*S*)-Rh2 showed no significant intracellular bactericidal effect. Therefore, 20(*S*)-Rh2 has a sensitizing mechanism to LVF in killing intracellular bacteria. LVF uptake experiments showed that 20(*S*)-Rh2 increased the accumulation of LVF in THP-1 cells in a concentration- and time-dependent manner (Fig. 5d). This result suggested that the sensitizing mechanism of 20(*S*)-Rh2 towards LVF intracellular activity was related to an increase in intracellular LVF accumulation.

Next, the mechanism by which 20(*S*)-Rh2 changed LVF uptake properties at the cellular level was explored. The uptake of LVF at 4 °C was significantly higher than that at 37 °C, which indicated that energy-dependent efflux transporters were involved [55]. Moreover, the uptake of LVF by THP-1 macrophages at 37 °C was significantly increased by 20(*S*)-Rh2, while there was no significant effect at 4 °C (Fig. 5e). These data together suggested that 20(*S*)-Rh2 likely increased the intracellular accumulation of LVF by inhibiting an efflux transporter in the cell.

Three major multidrug-resistant efflux transporters are abundantly expressed on THP-1 macrophages and mediate the transport of many quinolones [56–58]. For example, upregulation of MRP2 expression levels caused pharmacokinetic changes in the quinolone antibiotic norfloxacin, including downregulation of accumulation speed and degree parameters (AUC, *k*, and C_{max}) [59]. Verapamil and cyclosporin A mainly inhibit P-gp. Ko143 and quercetin mainly inhibit BCRP. MK571 and sulfinpyrazone are recognized as inhibitors of MRP2. As shown in Fig. 5f, LVF is a substrate for all three major efflux transporters. Does 20(*S*)-Rh2 interact with these three transporters or only some of them? Since we previously demonstrated 20(*S*)-Rh2 to be a noncompetitive P-gp inhibitor, only BCRP- and MRP2-specific membrane vesicles were used for 20(*S*)-Rh2 inhibition assays. The results showed that 20(*S*)-Rh2 exhibited a moderate inhibitory effect on BCRP but had

Table 2. PK–PD model parameters.

	LVF (4 μg/mL)		LVF+ Rh2 (1 μM)		LVF+ Rh2 (5 μM)		LVF+ Rh2 (10 μM)	
	Mean	CV (%)	Mean	CV (%)	Mean	CV (%)	Mean	CV (%)
k	0.086	36	0.077	45	0.085	38	0.071	41
F_a ($\times 10^{-3}$)	10.5	21	14.3	25	17.6*	31	21.4**	28
EC_{50}	10.6	32	12.4	42	9.4	33	11.8	37
E_{max}	310	24	301	35	321	31	305	25

The significance is indicated by $^*P < 0.05$, $^{**}P < 0.01$, versus LVF single treatment group.

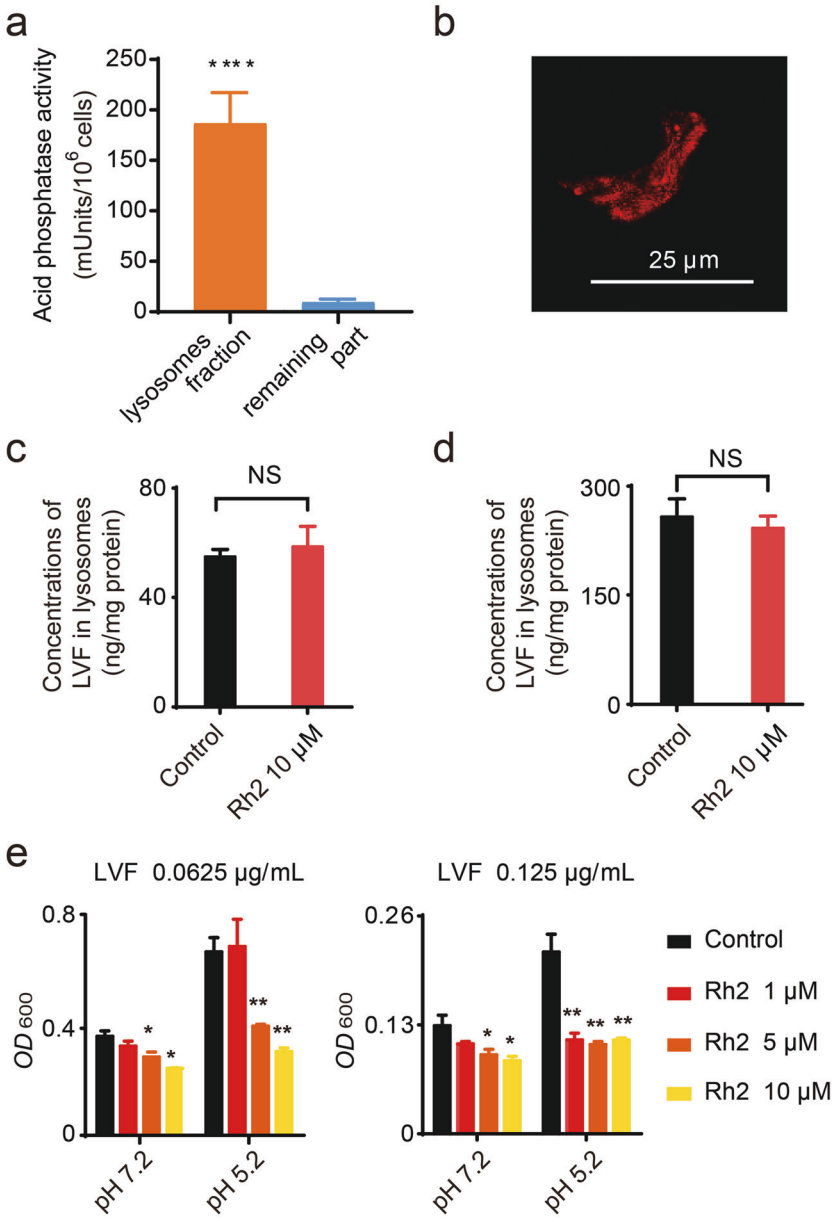

Fig. 7 20(S)-Rh2 had a stronger sensitizing effect towards LVF under lysosome-like acidic conditions. The prepared lysosomes were **a** identified by an acid phosphatase assay kit for its biomarker enzyme and **b** observed by a confocal laser scanning microscope for its staining with LysoTracker Red. **c** Cells were preincubated with 20(S)-Rh2 for 0.5 h followed by a further 2-h incubation in the presence of 16 μg/mL LVF, and then, lysosomes were separated, and the amount of LVF in lysosomes was determined. **d** Separated lysosomes were incubated in the presence of 20(S)-Rh2 and 8 μg/mL LVF for 20 min, and the amount of LVF in lysosomes was determined. **e** Effects of 20(S)-Rh2 on the bacteriostatic potency of LVF (0.0625 and 0.125 μg/mL) toward *S. aureus 25923* under different pH conditions. The data were the mean ± SEM, $n = 3$. The significance is indicated by $^{*}P < 0.05$, $^{**}P < 0.01$ versus the control.

Table 3. MIC and MBC of LVF to *S. aureus 25923* in different pH.

pH	MIC (μg/mL)	MBC (μg/mL)
7.2	0.5	2
5.2	1	4

no effect on MRP2 (Fig. 5g, h). Furthermore, 20(S)-Rh2 did not influence the expression of BCRP, MRP2, or P-gp after treatment for 24 h (Fig. 5i). Taken together, the increased intracellular accumulation of LVF was attributed to the functional inhibition of P-gp and BCRP by 20(S)-Rh2.

Based on the data above, a PK–PD model was developed with the purpose of quantitatively revealing the enhancing role of 20(S)-Rh2 in sensitizing LVF from a kinetics perspective. The parameters indicated that 20(S)-Rh2 did not change the inherent properties of LVF, as neither the uptake transport constant k of LVF across the cell membrane nor the efficacy of LVF itself (E_{max} and EC_{50}) was altered significantly. Instead, 20(S)-Rh2 changed the F_a properties of the cell.

Since *S. aureus 25923* ultimately accumulates in lysosomes after entering cells, lysosomes are an important site for the intracellular action of LVF [60, 61]. Hence, our research further moved to the subcellular level. It was found that 20(S)-Rh2 did not specifically increase the accumulation of LVF in lysosomes (Fig. 7c, d),

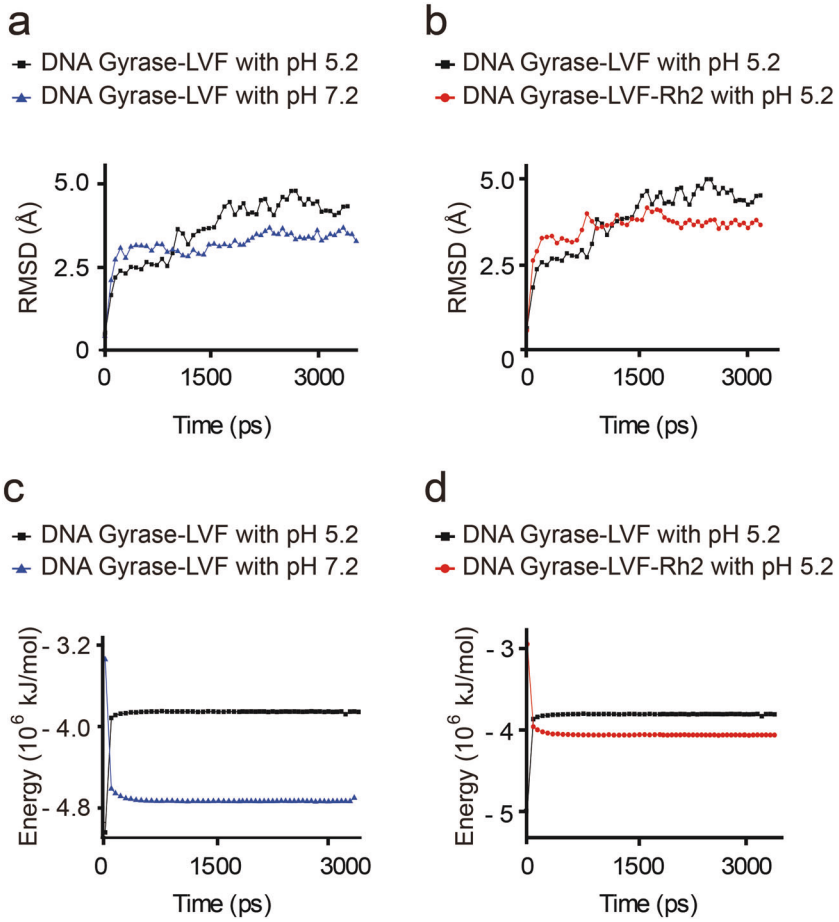

Fig. 8 20(*S*)-Rh2 enhanced the subcellular stability of LVF based on molecular dynamics simulation. RMSD change of the system during kinetic simulation: **a** different pH values, **b** presence or absence of 20(*S*)-Rh2 at pH 5.2. Energy change of the system during kinetic simulation: **c** different pH values, **d** presence or absence of 20(*S*)-Rh2 at pH 5.2.

suggesting that the sensitization of 20(*S*)-Rh2 towards LVF was not mediated by increasing the accumulation of LVF in lysosomes. Since the lysosome is an acidic compartment in the cell (pH 5.2), the bactericidal ability of LVF in an acidic environment, which simulates the lysosomal environment, was investigated. The bactericidal ability of LVF under acidic conditions was significantly weakened (Table 3), suggesting that the low pH in lysosomes might cause the poor intracellular efficacy of LVF [62]. Quinolone might bind to components such as intracellular proteins and lipids in a lysosomal acidic environment, and exposure of *S. aureus 25923* to acidic pH modifies the expression level of ~400 genes in a similar way to heat shock or behavior in biofilms [63].

Moreover, the interactions of 20(*S*)-Rh2 with LVF at different pH values showed that the enhancing effect of 20(*S*)-Rh2 on LVF was much more significant in the simulated lysosomal environment (pH 5.2) (Fig. 7e). Therefore, a molecular simulation of LVF and DNA gyrase was performed. The inhibition of DNA synthesis by quinolones is due to the stabilization of the quinolone-DNA gyrase-DNA complex which normally transient breaks, and thus kills bacteria [64, 65]. MD simulations of DNA gyrase and ligand complex models in different pH environments were carried out by Amber V16 MD simulation software. The RMSD change and the energy change of the system showed that the DNA gyrase–LVF complex was much more unstable (had higher energy) at pH 5.2 than at pH 7.2 (Fig. 8a, c). When 20(*S*)-Rh2 was added to the system at pH 5.2, the energy decreased, and the complex changed from unstable to much more stable (Fig. 8b, d), which was similar to the situation at pH 7.2. These results revealed that 20(*S*)-Rh2 could not increase the accumulation of LVF in lysosomes but rather improved the stability of the DNA gyrase–LVF complex in an acidic environment in lysosomes. This phenomenon might contribute to the enhancing effect of 20(*S*)-Rh2 on LVF at the subcellular level.

CONCLUSION

In summary, this study elucidated the mechanisms by which 20(*S*)-Rh2 sensitizes LVF intracellular bactericidal activity from the perspective of cellular pharmacokinetics. As 20(*S*)-Rh2 itself exhibited no significant intracellular bactericidal effect, it sensitized LVF intracellular activity: on the one hand, 20(*S*)-Rh2 inhibited efflux transporters on the cells, increased the intracellular accumulation of LVF, and thus made the intracellular bacteria surrounded by adequate amounts of the drug; on the other hand, 20(*S*)-Rh2 improved the stability of the DNA gyrase–LVF complex in acidic environments and promoted the efficacy of LVF in lysosomes. Our research might provide scientific evidence for 20(*S*)-Rh2 and quinolone combination usage in the treatment of infection.

ACKNOWLEDGEMENTS

The authors sincerely thank the post-graduates in the Key Lab of Drug Metabolism and Pharmacokinetics (China Pharmaceutical University, Nanjing, China) for their kind assistance. This work was supported by the Six Talent Peaks Project in Jiangsu Province (2018YY-060), Sanming Project of Medicine in Shenzhen (SZSM201801060).

AUTHOR CONTRIBUTIONS

JWZ, GJW, and FZ designed research; XYC, FQ, YYW, and YS performed research; JWZ, GJW, and FQ contributed new reagents or analytic tools; XYC, YYW, KH, WBZ, and FZ analyzed data; XYC, JWZ, and YL wrote the paper.

ADDITIONAL INFORMATION

Competing interests: The authors declare no competing interests

REFERENCES

1. Rous PF, Jones S. The protection of pathogenic microorganisms by living tissues cells. J Exp Med. 1916;23:601–12.
2. Ko E, Park S, Lee J, Cui C, Hou J, Kim M, et al. Ginsenoside Rh2 ameliorates atopic dermatitis in NC/Nga mice by suppressing NF-kappaB-mediated thymic stromal lymphopoietin expression and T helper type 2 differentiation. Int J Mol Sci. 2019;20:6111.
3. Thwaites G, Gant EV. Are bloodstream leukocytes Trojan Horses for the metastasis of *Staphylococcus aureus*? Nat Rev Microbiol. 2011;9:215–22.
4. Carlier MB, Garcia-Luque I, Montenez JP, Tulkens PM, Piret J. Accumulation, release and subcellular localization of azithromycin in phagocytic and non-phagocytic cells in culture. Int J Tissue React. 1994;16:211–20.
5. Seral C, Carryn S, Tulkens PM, Van Bambeke F. Influence of P-glycoprotein and MRP efflux pump inhibitors on the intracellular activity of azithromycin and ciprofloxacin in macrophages infected by *Listeria monocytogenes* or *Staphylococcus aureus*. J Antimicrob Chemother. 2003;51:1167–73.
6. Bosse MJ, Gruber HE, Ramp WK. Internalization of bacteria by osteoblasts in a patient with recurrent, long-term osteomyelitis. A case report. J Bone Jt Surg Am. 2005;87:1343–7.
7. Clement S, Vaudaux P, Francois P, Schrenzel J, Huggler E, Kampf S, et al. Evidence of an intracellular reservoir in the nasal mucosa of patients with recurrent *Staphylococcus aureus* rhinosinusitis. J Infect Dis. 2005;192:1023–8.
8. Jarry TM, Memmi G, Cheung AL. The expression of alpha-haemolysin is required for *Staphylococcus aureus* phagosomal escape after internalization in CFT-1 cells. Cell Microbiol. 2008;10:1801–14.
9. Que YA, Haefliger JA, Piroth L, François P, Widmer E, Entenza JM, et al. Fibrinogen and fibronectin binding cooperate for valve infection and invasion in *Staphylococcus aureus* experimental endocarditis. J Exp Med. 2005;201:1627–35.
10. Van Bambeke F, Barcian Macay M, Lemaire S, Tulkens PM. Cellular pharmacodynamics and pharmacokinetics of antibiotics: current views and perspectives. Curr Opin Drug Discov Devel. 2006;9:218–30.
11. Zhang H, Park S, Huang H, Kim E, Yi J, Choi S, et al. Anticancer effects and potential mechanisms of ginsenoside Rh2 in various cancer types (Review). Oncol Rep. 2021;45:33.
12. Lu H, Yuan X, Zhang Y, Han M, Liu S, Han K, et al. HCBP6 deficiency exacerbates glucose and lipid metabolism disorders in non-alcoholic fatty liver mice. Biomed Pharmacother. 2020;129:110347.
13. Chen X, Xu T, Lv X, Zhang J, Liu S. Ginsenoside Rh2 alleviates ulcerative colitis by regulating the STAT3/miR-214 signaling pathway. J Ethnopharmacol. 2021;274:113997.
14. Han M, Kim D. Effects of red and fermented Ginseng and Ginsenosides on allergic disorders. Biomolecules. 2020;10:634.
15. Zhang J, Zhou F, Wu X, Gu Y, Ai H, Zheng Y, et al. 20(*S*)-ginsenoside Rh2 non-competitively inhibits P-glycoprotein in vitro and in vivo: a case for herb-drug interactions. Drug Metab Dispos. 2010;38:2179–87.
16. Zhang J, Zhou F, Wu X, Zhang X, Chen Y, Zha BS, et al. Cellular pharmacokinetic mechanisms of adriamycin resistance and its modulation by 20(*S*)-ginsenoside Rh2 in MCF-7/Adr cells. Br J Pharmacol. 2012;165:120–34.
17. Zhang J, Sun Y, Wang Y, Lu M, He J, Liu J, et al. Non-antibiotic agent ginsenoside 20(*S*)-Rh2 enhanced the antibacterial effects of ciprofloxacin in vitro and in vivo as a potential NorA inhibitor. Eur J Pharmacol. 2014;740:277–84.
18. Shi G, Chen X, Wang H, Wang S, Guo X, Zhang X. Activity of sitafloxacin against extracellular and intracellular *Staphylococcus aureus* in vitro and in vivo: comparison with levofloxacin and moxifloxacin. J Antibiot. 2012;65:229–36.
19. Brinch KS, Sandberg A, Baudoux P, Van Bambeke F, Tulkens PM, Frimodt-Møller N, et al. Plectasin shows intracellular activity against *Staphylococcus aureus* in human THP-1 monocytes and in a mouse peritonitis model. Antimicrob Agents Chemother. 2009;53:4801–8.
20. Sandberg AJ, Hessler HR, Skov RL, Blom J, Frimodt-Møller N. Intracellular activity of antibiotics against *Staphylococcus aureus* in a mouse peritonitis model. Antimicrob Agents Chemother. 2009;53:1874–83.
21. Nguyen HA, Grellet J, Paillard D, Dubois V, Quentin C, Saux MC. Factors influencing the intracellular activity of fluoroquinolones: a study using levofloxacin in a *Staphylococcus aureus* THP-1 monocyte model. J Antimicrob Chemother. 2006;57:883–90.
22. Frimodt-Moller N. The mouse peritonitis model: present and future use. J Antimicrob Chemother. 1993;31:55–60.
23. Hao H, Cao L, Jiang C, Che Y, Zhang S, Takahashi S, et al. Farnesoid X receptor regulation of the NLRP3 inflammasome underlies cholestasis-associated sepsis. Cell Metab. 2017;25:856–67.
24. Seral C, Van Bambeke F, Tulkens PM. Quantitative analysis of gentamicin, azithromycin, telithromycin, ciprofloxacin, moxifloxacin, and oritavancin (LY333328) activities against intracellular *Staphylococcus aureus* in mouse J774 macrophages. Antimicrob Agents Chemother. 2003;47:2283–92.
25. Wen T, Yang A, Wang T, Jia M, Lai X, Meng J, et al. Ultra-small platinum nanoparticles on gold nanorods induced intracellular ROS fluctuation to drive megakaryocytic differentiation of leukemia cells. Biomater Sci. 2020;8:6204–11.
26. Chen Q, Chen H, Wang W, Liu J, Liu W, Ni P, et al. Glycyrrhetic acid, but not glycyrrhizic acid, strengthened entecavir activity by promoting its subcellular distribution in the liver via efflux inhibition. Eur J Pharm Sci. 2017;106:313–27.
27. Asadollahi P, Farahani NN, Mirzaii M, Khoramrooz SS, van Belkum A, Asadollahi K, et al. Distribution of the most prevalent spa types among clinical isolates of methicillin-resistant and susceptible *Staphylococcus aureus* around the World: a review. Front Microbiol. 2018;9:163.
28. Diekema DJ, Pfaller MA, Schmitz FJ, Smayevsky J, Bell J, Jones RN, et al. Survey of infections due to Staphylococcus species: frequency of occurrence and antimicrobial susceptibility of isolates collected in the United States, Canada, Latin America, Europe, and the Western Pacific region for the SENTRY Antimicrobial Surveillance Program, 1997-1999. Clin Infect Dis. 2001;32:S114–32.
29. Zloch M, Pomastowski P, Maslak E, Monedeiro F, Buszewski B. Study on molecular profiles of *Staphylococcus aureus* strains: spectrometric approach. Molecules. 2020;25:4893.
30. Sinha B, Herrmann M, Krause KH. Is *Staphylococcus aureus* an intracellular pathogen? Trends Microbiol. 2000;8:343–4.
31. Rogers D, Tompsett ER. The survival of staphylococci within human leukocytes. J Exp Med. 1952;95:209–30.
32. Kapral FA, Shayegani MG. Intracellular survival of staphylococci. J Exp Med. 1959;110:123–38.
33. Gresham HD, Lowrance JH, Caver TE, Wilson BS, Cheung AL, Lindberg FP. Survival of *Staphylococcus aureus* inside neutrophils contributes to infection. J Immunol. 2000;164:3713–22.
34. Maurin M, Raoult D. Use of aminoglycosides in treatment of infections due to intracellular bacteria. Antimicrob Agents Chemother. 2001;45:2977–86.
35. Monteiro KLC, de Aquino TM, Junior FJBM. An update on *Staphylococcus aureus* NorA efflux pump inhibitors. Curr Top Med Chem. 2020;20:2168–85.
36. Stubbings W, Leow P, Yong GC, Goh F, Körber-Irrgang B, Kresken M, et al. In vitro spectrum of activity of finafloxacin, a novel, pH-activated fluoroquinolone, under standard and acidic conditions. Antimicrob Agents Chemother. 2011;55:4394–7.
37. Wang G, Brunel J, Bolla J, Van Bambeke F. Pseudomonas aeruginosa the polyaminoisoprenyl potentiator NV716 revives old disused antibiotics against intracellular forms of infection by. Antimicrobial Agents Chemother. 2021;65: e02028–02020.
38. Peyrusson F, Butler D, Tulkens PM, Van Bambeke F. Cellular pharmacokinetics and intracellular activity of the novel peptide deformylase inhibitor GSK1322322 against *Staphylococcus aureus* laboratory and clinical strains with various resistance phenotypes: studies with human THP-1 monocytes and J774 murine macrophages. Antimicrob Agents Chemother. 2015;59:5747–60.
39. Imbuluzqueta E, Lemaire S, Gamazo C, Elizondo E, Ventosa N, Veciana J, et al. Cellular pharmacokinetics and intracellular activity against *Listeria monocytogenes* and *Staphylococcus aureus* of chemically modified and nanoencapsulated gentamicin. J Antimicrob Chemother. 2012;67:2158–64.
40. Peyrusson F, Tulkens PM, Van Bambeke F. Cellular pharmacokinetics and intracellular activity of Gepotidacin against *Staphylococcus aureus* isolates with different resistance phenotypes in models of cultured phagocytic cells. Antimicrob Agents Chemother. 2018;62:e02245–02217.
41. Sinha B, François PP, Nüsse O, Foti M, Hartford OM, Vaudaux P, et al. Fibronectin-binding protein acts as *Staphylococcus aureus* invasin via fibronectin bridging to integrin alpha5beta1. Cell Microbiol. 1999;1:101–17.
42. Patel S, Mathivanan N, Goyal A. Bacterial adhesins, the pathogenic weapons to trick host defense arsenal. Biomed Pharmacother. 2017;93:763–71.
43. Madani A, Garakani K, Mofrad MRK. Molecular mechanics of *Staphylococcus aureus* adhesin, CNA, and the inhibition of bacterial adhesion by stretching collagen. PLoS ONE. 2017;12:e0179601.
44. Garcia LG, Lemaire S, Kahl BC, Becker K, Proctor RA, Denis O, et al. Pharmacodynamic evaluation of the activity of antibiotics against hemin- and menadione-dependent small-colony variants of *Staphylococcus aureus* in models of

extracellular (broth) and intracellular (THP-1 monocytes) infections. Antimicrob Agents Chemother. 2012;56:3700–11.
45. Herman Bausier P, Valotteau C, Pietrocola G, Rindi S, Alsteens D, Foster TJ, et al. Mechanical strength and inhibition of the *Staphylococcus aureus* collagen-binding protein CNA. mBio. 2016;7:e01529–01516.
46. Barcia Macay M, Seral C, Mingeot Leclercq MP, Tulkens PM, Van Bambeke F. Pharmacodynamic evaluation of the intracellular activities of antibiotics against *Staphylococcus aureus* in a model of THP-1 macrophages. Antimicrob Agents Chemother. 2006;50:841–51.
47. Wang X, Wang X, Teng D, Mao R, Hao Y, Yang N, et al. Increased intracellular activity of MP1102 and NZ2114 against *Staphylococcus aureus* in vitro and in vivo. Sci Rep. 2018;8:4204.
48. Fraunholz M, Sinha B. Intracellular *Staphylococcus aureus*: live-in and let die. Front Cell Infect Microbiol. 2012;2:43.
49. Yang X, Shi G, Guo J, Wang C, He Y. Exosome-encapsulated antibiotic against intracellular infections of methicillin-resistant *Staphylococcus aureus*. Int J Nanomed. 2018;13:8095–104.
50. Carryn S, Chanteux H, Seral C, Mingeot Leclercq MP, Van Bambeke F, Tulkens PM. Intracellular pharmacodynamics of antibiotics. Infect Dis Clin North Am. 2003;17:615–34.
51. Zhang J, Lu M, Zhou F, Sun H, Hao G, Wu X, et al. Key role of nuclear factor-κB in the cellular pharmacokinetics of adriamycin in MCF-7/Adr cells: the potential mechanism for synergy with 20(*S*)-ginsenoside Rh2. Drug Metab Dispos. 2012;40:1900–8.
52. Zhang J, Zhou F, Lu M, Ji W, Niu F, Zha W, et al. Pharmacokinetics-pharmacology disconnection of herbal medicines and its potential solutions with cellular pharmacokinetic-pharmacodynamic strategy. Curr Drug Metab. 2012;13:558–76.
53. Stavri M, Piddock LJ, Gibbons S. Bacterial efflux pump inhibitors from natural sources. J Antimicrob Chemother. 2007;59:1247–60.
54. Lomovskaya O, Watkins W. Inhibition of efflux pumps as a novel approach to combat drug resistance in bacteria. J Mol Microbiol Biotechnol. 2001;3:225–36.
55. Verhalen B, Dastvan R, Thangapandian S, Peskova Y, Koteiche HA, Nakamoto RK, et al. Energy transduction and alternating access of the mammalian ABC transporter P-glycoprotein. Nature. 2017;543:738–41.
56. Daodee S, Wang Boonskul J, Jarukamjorn K, Sripanidkulchai B, Murakami T. Membrane transport of andrographolide in artificial membrane and rat small intestine. Pak J Biol Sci. 2007;10:2078–85.
57. Hayashi T, Abe F, Kato M, Saito H, Ueyama J, Kondo Y, et al. Involvement of sulfate conjugation and multidrug resistance-associated protein 2 (Mrp2) in sex-related differences in the pharmacokinetics of garenoxacin in rats. J Infect Chemother. 2011;17:24–9.
58. Wang D, Wei YH, Zhou Y, Zhang GQ, Zhang F, Li YQ, et al. Pharmacokinetic variation of ofloxacin based on gender-related difference in the expression of multidrug resistance-associated protein (Abcc2/Mrp2) in rat kidney. Yao Xue Xue Bao. 2012;47:624–9.
59. Luo B, Wang R, Li W, Yang T, Wang C, Lu H, et al. Pharmacokinetic changes of norfloxacin based on expression of MRP2 after acute exposure to high altitude at 4300m. Biomed Pharmacother. 2017;89:1078–85.
60. Winchell CG, Steele S, Kawula T, Voth DE. Dining in: intracellular bacterial pathogen interplay with autophagy. Curr Opin Microbiol. 2016;29:9–14.
61. Omotade TO, Roy CR. Manipulation of host cell organelles by intracellular pathogens. Microbiol Spectr. 2019;7:BAI-0022-2019.
62. Emrich NC, Heisig A, Stubbings W, Labischinski H, Heisig P. Antibacterial activity of finafloxacin under different pH conditions against isogenic strains of Escherichia coli expressing combinations of defined mechanisms of fluoroquinolone resistance. J Antimicrob Chemother. 2010;65:2530–3.
63. Baudoux P, Bles N, Lemaire S, Mingeot Leclercq MP, Tulkens PM, Van Bambeke F. Combined effect of pH and concentration on the activities of gentamicin and oxacillin against *Staphylococcus aureus* in pharmacodynamic models of extracellular and intracellular infections. J Antimicrob Chemother. 2007;59:246–53.
64. Tunitskaya VL, Khomutov AR, Kochetkov SN, Kotovskaya SK, Charushin VN. Inhibition of DNA gyrase by levofloxacin and related fluorine-containing heterocyclic compounds. Acta Nat. 2011;3:94–9.
65. Madurga S, Sánchez Céspedes J, Belda I, VilaE Giralt J. Mechanism of binding of fluoroquinolones to the quinolone resistance-determining region of DNA gyrase: towards an understanding of the molecular basis of quinolone resistance. Chembiochem. 2008;9:2081–6.